Iğdır Üniversitesi Fen Bilimleri Enstitüsü Dergisi, 11(4): 2772-2781, 2021
Journal of the Institute of Science and Technology, 11(4): 2772-2781, 2021

ISSN: 2146-0574, eISSN: 2536-4618

Fizik / Physics **DOI: 10.955530/jist.955530**

Araştırma Makalesi / *Research Article*

Geliş tarihi / Received: 21.06.2021 **Kabul tarihi / Accepted: 15.09.2021**

Atıf İçin: Çakır R, 2021. Polarization Effects on Intersubband Absorption in GaN/ZnGeN2 Quantum Wells. Journal of the Institute of Science and Technology, 11(4): 2772-2781.

To Cite: Çakır R, 2021. Polarization Effects on Intersubband Absorption in GaN/ZnGeN2 Quantum Wells. Journal of the Institute of Science and Technology, 11(4): 2772-2781.

Polarization Effects on Intersubband Absorption in GaN/ZnGeN2 Quantum Wells

Raşit ÇAKIR[1*]

ABSTRACT: The effects of spontaneous and piezoelectric polarizations on the intersubband absorption in the $GaN/ZnGeN_2$ quantum well are studied. Schrödinger and Poisson equations are solved self-consistently. The first order linear and third order nonlinear absorption coefficients of the intersubband transitions originating from ground and first excited states are calculated. We have presented the results relative to polarization, doping level and well length. The polarization causes the absorption peak to be reduced and shifted to higher energies, and the nonlinear absorption to become weaker, but this effect is slightly reversed with doping. The effect of polarization or doping increases with well length, but they are observed after 26 Å.

Keywords: Quantum well, GaN, $ZnGeN_2$, piezoelectric polarization, intersubband absorption.

[1]Raşit ÇAKIR (**Orcid ID:** 0000-0002-7104-9069), Recep Tayyip Erdoğan Üniversitesi, Fen Edebiyat Fakültesi, Fizik Bölümü, Rize, Türkiye

***Sorumlu Yazar/Corresponding Author:** Raşit ÇAKIR, e-mail: rasit.cakir@erdogan.edu.tr

INTRODUCTION

The Zn-IV-N_2 compounds, with the group-IV element Si, Ge, and Sn, have become of interest in recent years. They have potential benefits for photovoltaic applications (Punya and Lambrecht, 2013; Jaroenjittichai et al., 2017), and show promising results for optoelectronic applications (Punya et al., 2011). Their piezoelectric coefficients are comparable in magnitude to those in III-N materials (Paudel and Lambrecht, 2009; Paudel and Lambrecht, 2017), but they have more complex phonon structures (Paudel and Lambrecht, 2008; Paudel and Lambrecht, 2013). The $ZnGeN_2$ syntheses have been studied by several groups (Zhu et al., 1999; Du et al., 2008; Martinez et al., 2017; Häusler et al., 2017; Tellekamp et al., 2020). The electronic and elastic properties of $ZnGeN_2$ are similar to those of GaN (Chandra and Kumar, 1999). The calculations using the local density approximation and a GW correction by (Punya and Lambrecht, 2013; Jaroenjittichai et al., 2017) shows that the conduction band minimum of $ZnGeN_2$ is 1 eV higher than that of GaN, even though the hybrid density functional theory by (Adamski et al., 2020) shows different band alignment properties. The recent studies on the GaN/$ZnGeN_2$ quantum well have shown positive results. The donor binding energies of the GaN/$ZnGeN_2$ quantum well is studied by (Yıldırım, 2017). The scattering rate calculations by (Han et al., 2017) shows that the coupled quantum well structure of GaN/$ZnGeN_2$ is promising for the intersubband transitions in the near-IR. The GaN/$ZnGeN_2$ quantum multiwells can take high value of absorption coefficient (Laidouci et al., 2018).

Intersubband transitions in quantum wells, that is, the transitions between the states within the conduction band, have been the subject of extensive research, and are used in several devices such as infrared detectors, quantum cascade lasers and nonlinear waveguides for optical switching (Hofstetter et al., 2003; Hamazaki et al., 2004; Sun et al., 2005). The GaN/$ZnGeN_2$ quantum wells have large conduction band discontinuities, and can show intersubband transitions at short wavelengths. On the other hand, these materials have spontaneous and piezoelectric polarizations, which result in large interface charge densities, and the built-in electric filed can affect the intersubband transitions (Gunna et al., 2007).

To understand electronic and optical characteristics, a study on the electron states and the optical absorption is necessary. Various studies show that large optical nonlinearities as compared to the bulk material can be obtained because of the quantum confinement effects (Goldys EM and Shi JJ, 1998; Yılmaz S and Şahin M, 2010; Mora-Ramos ME et al., 2012). The purpose of this paper is to give such a description of intersubband optical absorption in the single GaN/$ZnGeN_2$ quantum well having the built-in electric field. The effect of incident optical intensity upon the nonlinear optical properties is studied. We investigate the intersubband optical absorption in the presence of optical radiation at the angular frequency ω and with polarization vector along z direction. We focus on the first order linear and third order nonlinear absorption coefficients, which were derived by using the density matrix formalism and perturbation expansion method by Ahn and Chuang, 1987. To the best of our knowledge, there is no report on the nonlinear optical properties of such a quantum well structure. Therefore it would be useful to study the linear and nonlinear optical properties of this structure.

We have studied the single GaN/$ZnGeN_2$ quantum well with spontaneous and piezoelectric polarizations and doping in the well, and obtained energy eigenvalues and eigenfunctions, dipole matrix elements, and the linear and the third order nonlinear optical intersubband absorption coefficients. The Schrödinger equation and the Poisson equation are discretized by means of finite differences and they are solved self-consistently. We have presented the results relative to well length, doping level and polarization.

MATERIALS AND METHODS

The Hamiltonian for the electrons inside the potential $U(z)$ within the effective mass and envelope function approximation is

$$H = -\frac{\hbar^2}{2m^*}\left(\frac{\partial^2}{\partial x^2}+\frac{\partial^2}{\partial y^2}+\frac{\partial^2}{\partial z^2}\right)+\ U(z) \tag{1}$$

where m^* is the effective mass and z is the growth direction. The potential term

$$U(z) = \Delta E_c(z) + U_\epsilon(z) - e\ V_H(z) \tag{2}$$

includes the conduction band offset $\Delta E_c(z)$, the strain induced contribution $U_\epsilon(z)$, and the Hartree potential $V_H(z)$, where $e = |e|$ is the elementary charge. The energy eigenvalues $E_{n,k}$ and eigenfunctions $\psi_{n,k}$ for this Hamiltonian are given as

$$E_{n,k} = E_n + \frac{\hbar^2}{2m^*}\left|\boldsymbol{k}_\parallel\right|^2 \tag{3}$$

$$\psi_{n,k}(\boldsymbol{r}) = \psi_n(z)\exp(i\ \boldsymbol{k}_\parallel \cdot \boldsymbol{r}_\parallel) \tag{4}$$

where $\boldsymbol{k}_\parallel$ and $\boldsymbol{r}_\parallel$ are the wave and position vectors in the xy plane, and E_n is the energy and $\psi_n(z)$ is the wave function of the nth subband in the growth direction (Flügge, 1971).

We solve numerically the Schrödinger equation

$$H_z\psi_n(z) = -\frac{\hbar^2}{2}\frac{\partial}{\partial z}\frac{1}{m^*(z)}\frac{\partial}{\partial z}\psi_n(z) + \ U(z)\psi_n(z) = E_n\psi_n(z) \tag{5}$$

in the growth direction, where H_z is the z component of the Hamiltonian and $m^* = m^*(z)$ is position dependent. Potential due to the strain is

$$U_\epsilon = \ 2\ \epsilon_1\left(\ a_{c\perp} - a_{c\parallel}\frac{C_{13}}{C_{33}}\right) \tag{6}$$

where ϵ_1 is in-plane strain, $a_{c\perp}$ and $a_{c\parallel}$ are deformation potential constants, and C_{13} and C_{33} are elastic stiffness constants. The in-plane strain is

$$\epsilon_1 = \frac{a_0 - \ a_l}{a_l} \tag{7}$$

where a_0 and a_1 are the lattice constants of the substrate and the material grown.

To get the Hartree potential $V_H(z)$, we solve the Poisson equation

$$\frac{\partial}{\partial z}\varepsilon(z)\frac{\partial}{\partial z}V_H(z) = -\rho(z) \tag{8}$$

where the permittivity $\varepsilon(z) = \varepsilon_0\varepsilon_r(z)$ depends on the position. The volume charge density

$$\rho(z) = \ e\ N_D(z) - e\ n(z) + \rho_{pol}(z) \tag{9}$$

includes the doping density $N_D(z)$, the electron density $n(z)$, and the polarization volume density $\rho_{pol}(z)$. The electron density is obtained by

$$n(z) = \sum_n \frac{k_B T}{\pi\hbar^2}m^*(z)\ln\left[1+\exp\left(\frac{E_F - E_n}{k_B T}\right)\right]|\psi_n(z)|^2 \tag{10}$$

where the wave functions ψ_n are obtained from the Schrödinger equation, the summation is over the energy levels, E_F is the Fermi energy, k_B is the Boltzmann constant and T is temperature. Polarization volume density is

$$\rho_{pol}(z) = -\frac{\partial P}{\partial z} \tag{11}$$

where $P(z) = P_{SP}(z) + P_{PZ}(z)$ is the total polarization due to the spontaneous polarization and piezoelectric polarization, respectively. The piezoelectric polarization in the growth direction in a wurtzite layer under biaxial strain is

$$P_{PZ} = 2\,\epsilon_1\left(e_{31} - e_{33}\frac{C_{13}}{C_{33}}\right) \tag{12}$$

where e_{31} and e_{33} are the piezoelectric constants (Harrison and Jovanović, 2016).

The first order linear and third order nonlinear absorption coefficients are given, respectively, as

$$\alpha^{(1)} = \frac{\omega}{n_r c\varepsilon_0}|\mu_{10}|^2\frac{\sigma_s\hbar\Gamma_0}{(E_{10}-\hbar\omega)^2+(\hbar\Gamma_0)^2} \tag{13}$$

$$\alpha^{(3)} = -2\omega\left(\frac{1}{n_r c\varepsilon_0}\right)^2|\mu_{10}|^4\frac{I\sigma_s\hbar\Gamma_0}{[(E_{10}-\hbar\omega)^2+(\hbar\Gamma_0)^2]^2} \times\left\{1-\frac{|\mu_{11}-\mu_{00}|^2}{4|\mu_{10}|^2}\frac{(E_{10}-\hbar\omega)^2-(\hbar\Gamma_0)^2+2E_{10}(E_{10}-\hbar\omega)}{E_{10}^2+(\hbar\Gamma_0)^2}\right\} \tag{14}$$

where $|\mu_{ij}| = e|\langle\psi_i|z|\psi_j\rangle|$, $(i,j=0,1)$, are the dipole matrix elements, $E_{10}=E_1-E_0$ is the energy difference, σ_s is the electron density in the well, Γ_0 is the inverse of the relaxation time, $n_r=\sqrt{\varepsilon_r}$ is the refractive index of the well, I is the intensity of the incident light having the frequency of ω, ε_0 is the vacuum permittivity, and c is the speed of light in vacuum (Ahn and Chuang, 1987; Yıldırım and Tomak, 2005; Boyd, 2020).

RESULTS AND DISCUSSION

The potential energy profile of the GaN/$ZnGeN_2$ quantum well and the squared electronic wave functions of the ground and first excited states are shown in Figure 1(a) for the well length of $L_w = 50$ Å and for the doping density of $N_D = 2\times10^{24}$ m^{-3} in the well and zero in the barriers. Each barrier is taken as 400 Å in all calculations. The conduction band minimum of GaN is 1 eV less than that of $ZnGeN_2$ (Jaroenjittichai et al., 2017). The parameters used in the calculations can be seen in Table 1. The GaN parameters are from Piprek J, 2007 and the $ZnGeN_2$ parameters are from Jaroenjittichai et al., 2017; Punya et al., 2011; Punya A, Lambrecht WRL, 2013; Paudel TR, Lambrecht WRL, 2008; Paudel TR, Lambrecht WRL, 2009. Because deformation potential constants of $ZnGeN_2$ are not available, those of GaN are used in the calculations instead. The effect of the doping is a small curvature in the well, which is hardly seen in the figure, while the polarization causes the potential to be inclined. The curvatures due to doping can be seen clearly in another potential profile in Figure 2(b), drawn for various doping values.

We consider the wurtzite GaN grown on the orthorhombic $ZnGeN_2$ thick layer in the [0001] direction at $T = 300$ K. We take half of the lattice constant of $ZnGeN_2$ as explained in (Adamski et al., 2020). The well is under tensile strain since $\epsilon_1 = 0.00031 > 0$ and its piezoelectric polarization is $P_{PZ} = -0.00032$ C m^{-2} in the growth direction while the barriers are unstrained and without piezoelectric polarization. The well and the barriers have also their spontaneous polarization values as seen in Table 1.

The electric field and the areal charge density in Figure 1(b) are calculated from $U(z)$ in Eq. (2) as $F = 1/e\,(dU/dz)$ and $\delta\sigma = \rho\delta z = \varepsilon/e\,(d^2U/dz^2)\delta z$ since ΔE_c, which equals 1 eV on the barriers and zero on the well, and U_ϵ, which equals -3.35 meV on the well and zero on the barriers, are constants except the boundaries. The curvature on the electric field happens due to the doping, and so the charge in the figure is caused by the doping only. The electric field value due to the total polarization only are seen as dashed blue lines in the figure, which are $F_b = -0.72\times10^7$ V m^{-1} in the barriers and $F_w = 11.5610^7$ V m^{-1} in the well. The charges due to the total polarization are on the boundaries only, and they have high values as $\pm706.75\times10^{14}$ e m^{-2}, which cannot be seen on the graph.

Table 1. Material Properties of GaN and $ZnGeN_2$

Properties	**Symbol (unit)**	**GaN**	**$ZnGeN_2$**
Energy gap	E_g (eV)	3.51	3.4
Lattice constant	a_l (Å)	3.189	6.38
Effective mass ratio	m^*/m_0	0.20	0.15
Dielectric constant	ε_r	10.4	10.61
Spontaneous polarization	P_{SP} (C m^{-2})	-0.0339	-0.023
Elastic stiffness constants			
	C_{13} (GPa)	106	103
	C_{33} (GPa)	398	401
Piezoelectris constants			
	e_{31} (C m^{-2})	-0.338	-0.43
	e_{33} (C m^{-2})	0.667	0.73
Deformation potential constants			
in growth plane	$a_{c\perp}$ (eV)	-8.2	-8.2
in growth direction	$a_{c\parallel}$ (eV)	-10.7	-10.7

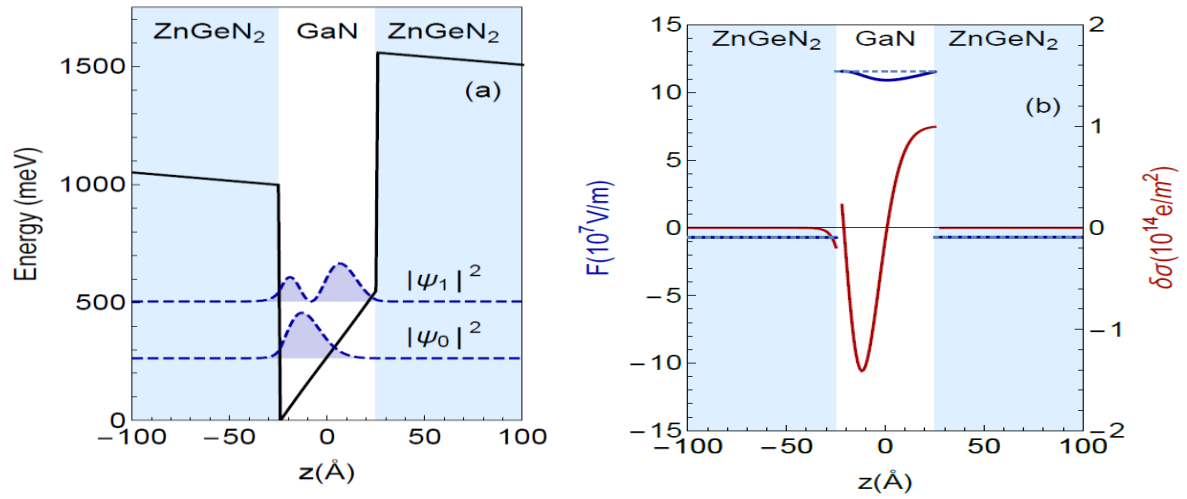

Figure 1. a) The squared electronic wave functions (dashed blue) of the ground and first excited states on the quantum well potential (black), b) the total electric field strength F (solid blue), the electric field value due to the total polarization only (dashed blue), and the areal charge density δσ (red), for the well length of 50 Å and the doping density of 2×10^{24} m^{-3} in the well

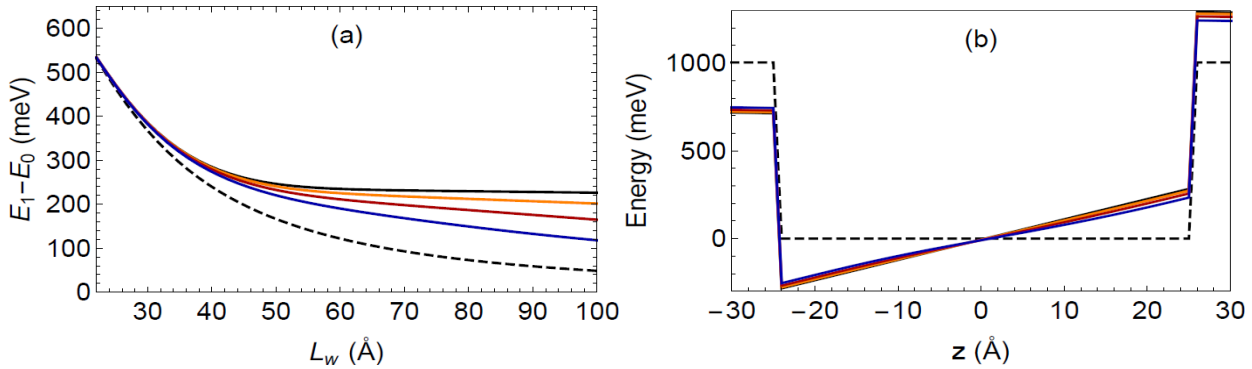

Figure 2. a) The energy difference values between the ground and first excited states $E_1 - E_0$ relative to the well length and b) the potential profiles for the well length $L_w = 50$ Å, for the well without polarization or doping (dashed), with polarization but without doping (black), and with polarization and the doping values of 2×10^{24} m^{-3} (orange), 5×10^{24} m^{-3} (red) and 10^{25} m^{-3} (blue)

The energy differences between ground and first excited states relative to the well length can be seen in Figure 2(a) for the doping values of 2×10^{24} m^{-3}, 5×10^{24} m^{-3} and 10^{25} m^{-3}, additionally for the finite square well (without polarization or doping) and for the triangular well (with polarization only). We can see the effects of polarization and doping on the well potentials in Figure 2(b), and compare these effects with the energy differences. Until the well length of $L_w = 22$ Å, the first excited state wave function is not confined in the well so we have started the well length from that value. From 22 Å to 26 Å, the ground state energy is above the band edge so the energy differences are not affected by the triangular shape and they do not differ from that of the finite square well. Greater than 26 Å, the ground state wave functions position in the triangular region of the potential and these values start to differ. In the triangular potential without doping, the energy difference value reaches a constant value, because the ground and first excited state wave functions do not touch the right interface and they see the same triangular potential shape as the well width increases. However, the energy differences of the doped wells are not constant, and their values differ from each other because of the curvatures on the well bottom.

Figure 3 shows the dipole matrix elements $|\mu_{ij}|$ of the ground and first excited states for the same doping values, and also comparing them with the finite square and triangular wells. The polarization clearly changes the values of the dipole matrix elements, and so reduces the magnitude of $|\mu_{01}|$, even though the doping slightly reduces this effect. When there is doping without any polarization, there is no visible change in the energy difference and the dipole matrix elements from those of the finite square well, which are not shown in the figures, so we can say that these effects are due to the polarization only.

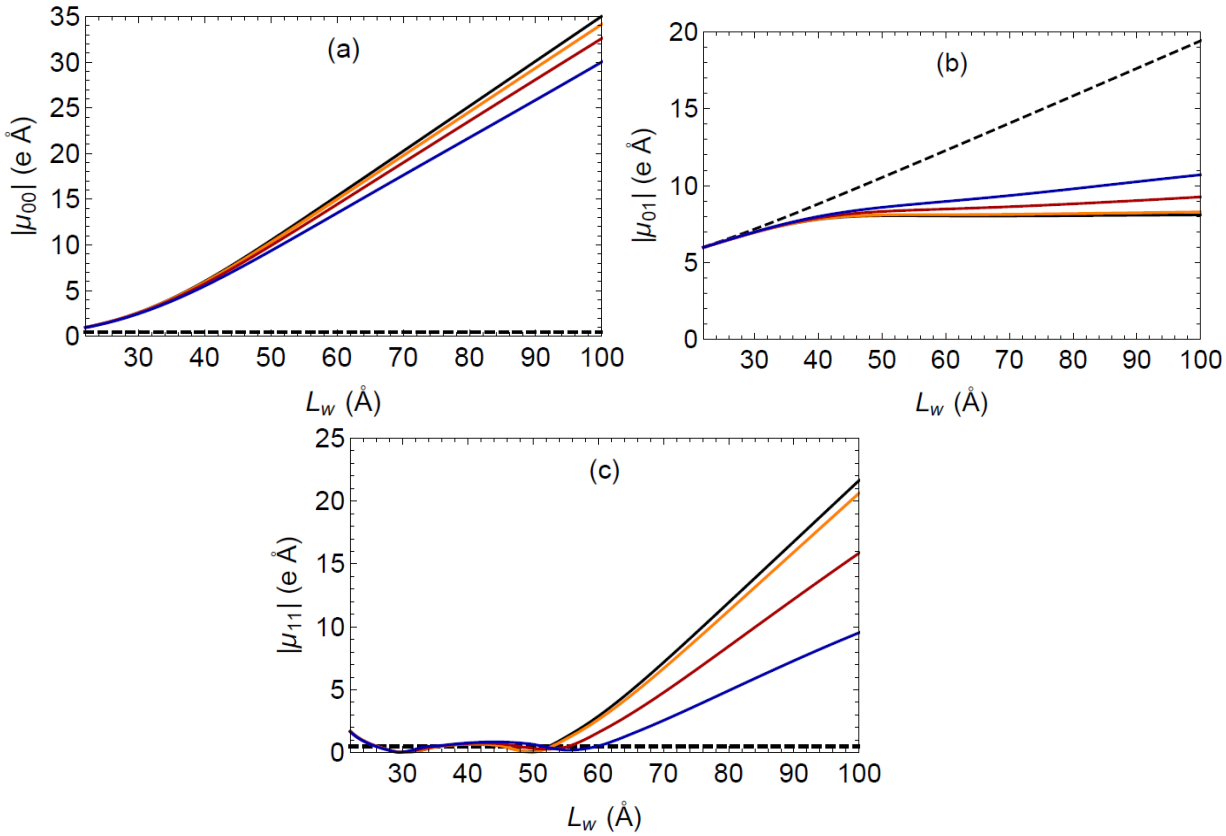

Figure 3. The dipole matrix elements, a) $|\mu_{00}|$, b) $|\mu_{01}|$ and c) $|\mu_{11}|$ between the ground and first excited states, for the well without polarization or doping (dashed), with polarization but without doping (black), and with with polarization and the doping values of 2×10^{24} m^{-3} (orange), 5×10^{24} m^{-3} (red) and 10^{25} m^{-3} (blue)

For the calculations of the absorption coefficients, we used $I = 10^{10}$ W m^2, $n_r = \sqrt{10.4}$ and σ_s as the doping density. In Figure 4 and Figure 5, we can see the total absorption coefficients $\alpha = \alpha^{(1)} + \alpha^{(3)}$ together with the nonlinear coefficients $\alpha^{(3)}$ for $\hbar\Gamma_0 = 60$ meV. The nonlinear contribution of $\alpha^{(3)}$ is negligible since it is much smaller than $\alpha^{(1)}$ and so we get $\alpha \approx \alpha^{(1)}$. Figure 4 shows the absorption for the electron densities σ_s of 2×10^{24} m^{-3}, 5×10^{24} m^{-3} and 10^{25} m^{-3}, and for the well lengths L_w of 25 Å, 50 Å, 75 Å and 100 Å. The absorption peak shifts to lower energies as the well length or doping increases, since the energy difference values decrease. The peak values are at the $\hbar\omega = E_{10}$ energy values of the corresponding well length as seen in Figure 2(a). We also consider the case with total polarization and the case without any polarization in Figure 5, showing the absorption for the electron density of $\sigma_s = 2 \times 10^{24}$ m^{-3} and for the same L_w values as before. The peak values of the total absorption decrease and shift to higher energies due to the polarization, and the nonlinear absorption is reduced greatly. However, these effects are hardly seen for the case of $L_w = 20$ Å because, until 26 Å, the wave functions behave like the square well wave functions as explained before. The dependency on Γ_0 is obvious in Eq. (13) and (14). The absorption peak value decreases and the curve expands as Γ_0 increases.

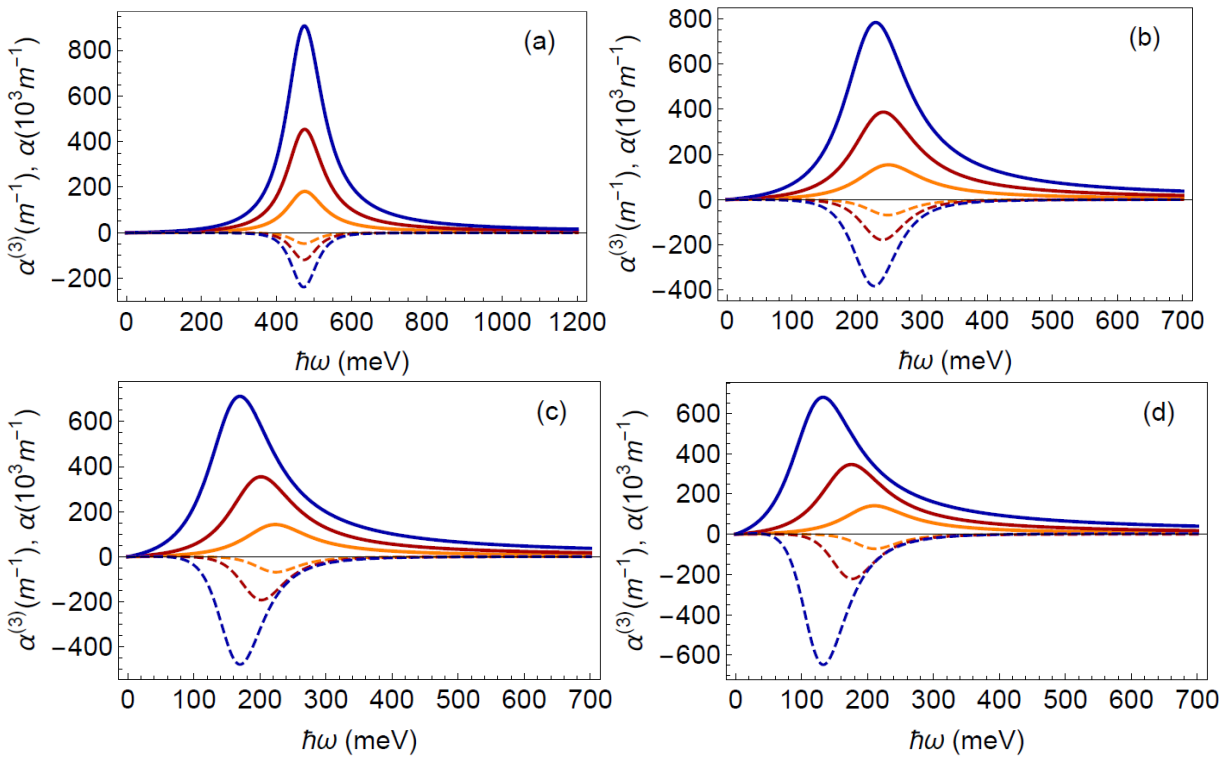

Figure 4. The total absorption coefficients α (solid lines) and $\alpha^{(3)}$ (dashed lines) relative to the incident light energy $\hbar\omega$ for $\hbar\Gamma_0 = 60$ meV, for the electron densities σ_s of 2×10^{24} m^{-3} (orange), 5×10^{24} m^{-3} (red) and 10^{25} m^{-3} (blue), and for the well lengths L_w of a) 25 Å, b) 50 Å c) 75 Å, and d) 100 Å

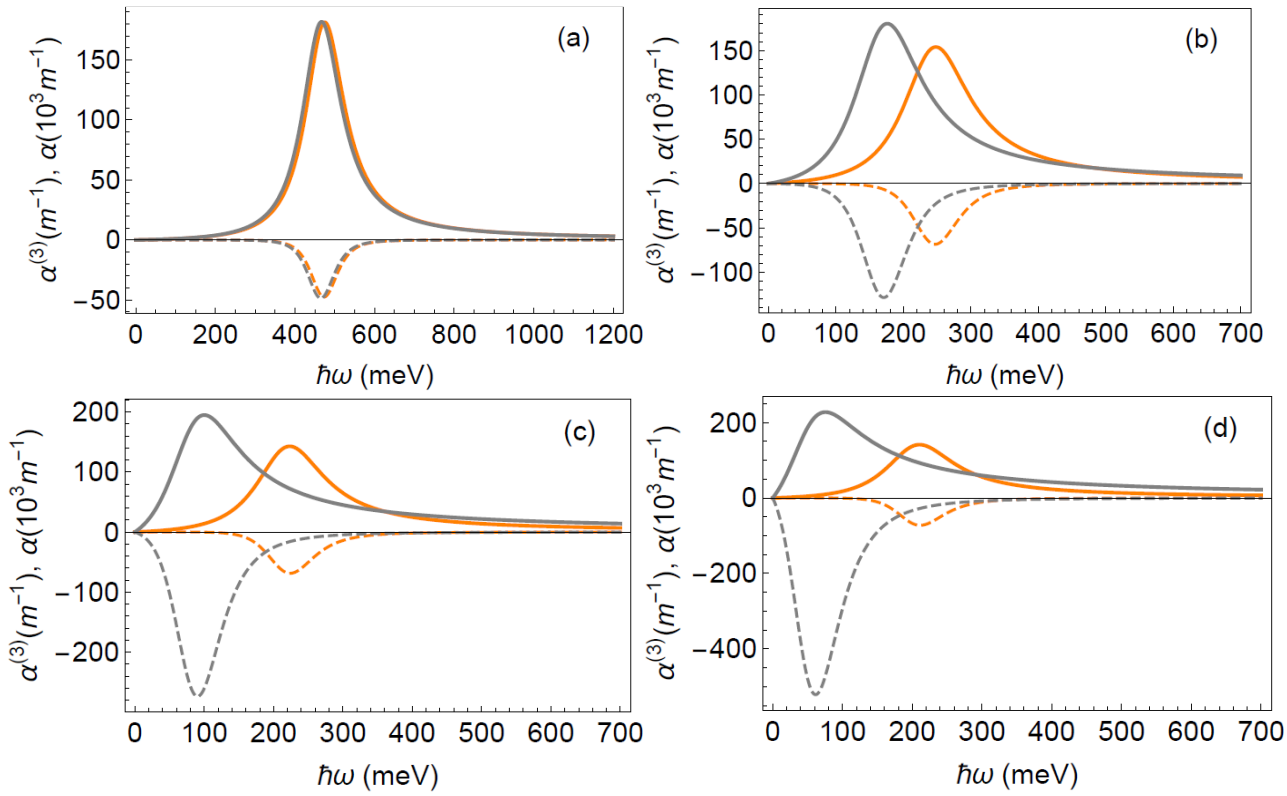

Figure 5. The total absorption coefficients α (solid lines) and $\alpha^{(3)}$ (dashed lines) relative to the incident light energy $\hbar\omega$ for $\hbar\Gamma_0 = 60$ meV, for the electron density σ_s of 2×10^{24} m^3 , with total polarization (orange) and without any polarization (gray), and for the well lengths L_w of a) 25 Å, b) 50 Å c) 75 Å, and d) 100 Å

CONCLUSION

We have studied the effects of piezoelectric and spontaneous polarizations on the GaN/ZnGeN$_2$ quantum well, as well as the effects of doping in the well. Polarization charges accumulated on the boundaries of the well and causes the potential to be inclined while doping charges are mainly in the well and makes the well bottom get curved. Their effects to the energy difference values and dipole matrix elements are minimum until the well length of $L_w = 26$ Å because they are not affected by the changes of the potential profile very much. After that length, the energy difference values get higher with the polarization and the intersubband transition rates drops, but doping reduces these effects to some extent. We also present the changes in the absorption coefficients. The total absorption is reduced and blue shifted due to the polarization, while doping can increase the absorption and red shifts it. Nonlinear absorption is reduced because of the polarization and its contribution to the absorption rate is minimal. We hope that these results can be useful for possible device applications based on GaN/ZnGeN$_2$ material.

REFERENCES

Adamski NL, Wickramaratne D, de Walle CGV, 2020. Band alignments and polarization properties of the Zn-IV-nitrides. Journal of Materials Chemistry C, 8:7890–7898.

Ahn D, Chuang SL, 1987. Calculation of linear and nonlinear intersubband optical absorptions in a quantum well model with an applied electric field. IEEE Journal of Quantum Electronics, 23(12):2196–2204.

Boyd RW, 2020. Nonlinear Optics (Fourth Edition), Elsevier.

Chandra S, Kumar V, 2019. Structural, electronic and elastic properties of $ZnGeN_2$ and WZ-GaN under different hydrostatic pressures: A first-principle study. International Journal of Modern Physics B, 33(25):1950297.

Flügge S, 1971. Practical Quantum Mechanics. Springer Berlin Heidelberg.

Goldys EM, Shi JJ, 1998. Linear and Nonlinear Intersubband Optical Absorption in a Strained Double Barrier Quantum Well. Physica Status Solidi B, 210, 237.

Gunna S, Bertazzi F, Paiella R, Bellotti E, 2007. Nitride Semiconductor Devices: Principles and Simulation. John Wiley & Sons Ltd. p117-143.

Hamazaki J, Matsui S, Kunugita H, Ema K, Kanazawa H, Tachibana T, Kikuchi A, Kishino K, 2004. Ultrafast intersubband relaxation and nonlinear susceptibility at 1.55 μm in GaN/AlN multiple-quantum wells. Applied Physics Letters, 84(2)1102–1104.

Han L, Lieberman C, Zhao H, 2017. Study of intersubband transitions in GaN-$ZnGeN_2$ coupled quantum wells. Journal of Applied Physics, 121(3):093101.

Harrison P, Jovanović VD, 2016. Quantum Wells Wires and Dots, John Wiley & Sons Ltd. p223-248.

Häusler J, Schimmel S, Wellmann P, Schnick W, 2017. Ammonothermal synthesis of earth-abundant nitride semiconductors $ZnSiN_2$ and $ZnGeN_2$ and dissolution monitoring by in situ X-ray imaging. Chemistry - A European Journal, 23(50):12275–12282.

Hofstetter D, Schad SS, Wu H, Schaff HW, Eastman LF, 2003. GaN/AlN-based quantum-well infrared photodetector for 1.55 μm. Applied Physics Letters, 83(7):572–574.

Jaroenjittichai AP, Lyu S, Lambrecht WRL, 2017. Erratum: Band offsets between $ZnGeN_2$, GaN, ZnO, and $ZnSnN_2$ and their potential impact for solar cells [Phys. Rev. B 88, 075302 (2013)]. Physical Review B, 96:079907.

Du K, Bekele C, Hayman CC, Angus JC, Pirouz P, Kash K, 2008. Synthesis and characterization of $ZnGeN_2$ grown from elemental Zn and Ge sources, Journal of Crystal Growth, 310(6), 1057–1061.

Laidouci A, Aissat A, Vilcot JP, 2018. Temperature Effect on $ZnGeN_2$/GaN Multiwell Quantum Solar Cells. 6th International Renewable and Sustainable Energy Conference (IRSEC), 5-8 Dec. 2018, Rabat, Morocco.

Martinez AD, Fioretti AN, Toberer ES, Tamboli AC, 2017. Synthesis, structure, and optoelectronic properties of II-IV-V materials. Journal of Materials Chemistry A, 5:11418–11435.

Mora-Ramos ME, Duque CA, Kasapoğlu E, Sarı H, Sökmen I, 2012. Linear and nonlinear optical properties in a semiconductor quantumwell under intense laser radiation: Effects of applied electromagnetic fields. Journal of Luminescence, 132, 901–913.

Paudel TR, Lambrecht WRL, 2008. First-principles study of phonons and related ground-state properties and spectra in Zn-IV-N_2 compounds. Physical Review B, 78:1152024.

Paudel TR, Lambrecht WRL, 2009. First-principles calculations of elasticity, polarization-related properties, and nonlinear optical coefficients in Zn-IV-N_2 compounds. Physical Review B, 79:245205.

Paudel TR, Lambrecht WRL, 2013. Erratum: First-principles study of phonons and related ground-state properties and spectra in Zn-IV-N_2 compounds [Phys. Rev. B78, 115204 (2008)]. Physical Review B, 87:039901.

Paudel TR, Lambrecht WRL, 2017. Erratum: First-principles calculations of elasticity, polarization-related properties, and nonlinear optical coefficients in Zn-IV-N_2 compounds [Phys. Rev. B 79, 245205 (2009)]. Physical Review B, 96:079906.

Piprek J, 2007. Nitrite Semiconductor Devices, WILEY-VCH Verlag GmbH & Co. KGaA, pp. 24, 53, 58, Weinheim.

Punya A, Lambrecht WRL, van Schilfgaarde M, 2011. Quasiparticle band structure of Zn-IV-N_2 compounds. Physical Review B, 84:165204.

Punya A, Lambrecht WRL, 2013. Band offsets between $ZnGeN_2$, GaN, ZnO, and $ZnSnN_2$ and their potential impact for solar cells. Physical Review B, 88:075302.

Sun G, Soref RA, Khurgin JB, 2005. Active region design of a terahertz GaN/$Al_{0.15}Ga_{0.85}N$ quantum cascade laser. Superlattices and Microstructures, 37(2)107–113.

Tellekamp MB, Melamed LC, Norman AG, Tamboli A, 2020. Heteroepitaxial Integration of $ZnGeN_2$ on GaN Buffers Using Molecular Beam Epitaxy. Crystal Growth & Design, 20(3):1868–1875.

Yıldırım H, Tomak M, 2005. Nonlinear optical properties of a Pöschl-Teller quantum well. Physical Review B, 72:115340.

Yıldırım H, 2017. Donor binding energies in a GaN/$ZnGeN_2$ quantum well. Superlattices and Microstructures, 111(11):529–535.

Yılmaz S, Şahin M, 2010. Third-order nonlinear absorption spectra of an impurity in a spherical quantum dot with different confining potential. Physica Status Solidi B, 247, No. 2, 371–374.

Zhu LD, Maruska PH, Norris PE, Yip PW, Bouthillette LO, 1999. Epitaxial Growth and Structural Characterization of Single Crystalline $ZnGeN_2$. MRS Internet Journal of Nitride Semiconductor Research, 4:149–154.